Available online at www.sciencedirect.com
SCIENCE DIRECT®
International Journal of Heat and Mass Transfer 47 (2004) 589–599
International Journal of HEAT and MASS TRANSFER
www.elsevier.com/locate/ijhmt

Prediction of friction factors and heat transfer coefficients for turbulent flow in corrugated tubes combined with twisted tape inserts. Part 1: friction factors

Ventsislav Zimparov *

Gabrovo Technical University, 4 Hadji Dimitar Str., BG-5300 Gabrovo, Bulgaria

Received 5 February 2003

Abstract

A simple mathematical model following the suggestion of Smithberg and Landis has been created to predict the friction factors for the case of a fully developed turbulent flow in a spirally corrugated tube combined with a twisted tape insert. The flow field is divided into two principal regions—a helicoidal core flow modified by secondary circulation effects and a twisting boundary layer flow. The "wall roughness" has an effect simultaneously on the axial velocity, secondary fluid motion and the resulting swirl mixing. The model reflects the influence of the "wall roughness" on the axial and tangential velocity components. The calculated friction factors have been compared with 570 experimental points obtained from 57 tubes tested. Five hundred points (87.7%) have a relative difference of less than ±15%; fifty one points (8.9%) have a difference of within ±(15–20)% and only nineteen points (3.4%) have a relative difference greater than ±20%.

Keywords: Compound heat transfer; Corrugated tubes with twisted tape inserts; Friction factor; Single-phase turbulent flow

1. Introduction

The performance of conventional heat exchangers can be substantially improved by many augmentation techniques applied to the design systems. Heat transfer enhancement devices are commonly employed to improve the performance of an existing heat exchanger or to reduce the size and cost of a proposed heat exchanger. An alternative goal is to use such techniques to increase the system thermodynamic efficiency, which allows reducing the operating cost [1–3].

Enhancement techniques can basically be classified as passive methods, which require no direct application of external power, and active methods, which require external power. The enhancement of a single-phase flow is important because that flow usually represents the dominant thermal resistance in a two-fluid heat exchanger, especially if it is a gas (as compared to a liquid). Balaras [4] selects to group the augmentation methods for single-phase flow heat exchangers into three categories, based on whether the enhancement is caused by either the heat exchanger surface (surface methods), or the working fluid (fluid methods), or a combination of the two (combined methods).

Surface methods include any techniques which directly involve the heat exchanger surface. They are used on the side of the surface that comes into contact with a fluid of low heat transfer coefficient in order to reduce the thickness of the boundary layer and to introduce better fluid mixing. The primary mechanisms for thinning the boundary layer are increased stream velocity and turbulent mixing. Secondary recirculation flows can further enhance convective heat transfer. Flows from the core to the wall reduce the thickness of the boundary layer and the secondary flows from the wall to the core promote mixing. Flow separation and reattachment within the flow channel also contribute to heat transfer enhancement.

* Fax: +359-66-801155.
E-mail address: vdzim@tugab.bg (V. Zimparov).

0017-9310/$ - see front matter © 2003 Elsevier Ltd. All rights reserved.
doi:10.1016/j.ijheatmasstransfer.2003.08.003

Nomenclature

A	surface area (m^2)
D	tube diameter (m)
e	ridge height (m)
H	pitch of the twisted tape (m)
L	length of the tube (m)
l	mixing length (m)
$\dot{m}$	mass flow rate ($kg\,s^{-1}$)
p	pitch of ridging (m)
Δp	pressure drop (Pa)
r_0	tube radius (m)
U	axial velocity component ($m\,s^{-1}$)
u_*	shear velocity $(\tau_w/\rho)^{1/2}$ ($m\,s^{-1}$)
V	total velocity vector ($m\,s^{-1}$)
y	distance from the wall (m)

Greek symbols

β	helix angle of rib (°)
δ	thickness of the tape (m)
ε_m	eddy kinematic viscosity ($m^2\,s^{-1}$)
ν	kinematic viscosity ($m^2\,s^{-1}$)
ρ	fluid density ($kg\,m^{-3}$)
τ	shear stress (Pa)

Dimensionless groups

e_S^+	dimensionless equivalent sand grain roughness $(e_S u_*/\nu)$
f	fanning friction factor $(2\tau_w/(\rho U_m^2))$
l^+	dimensionless mixing length (lu_*/ν)
Re	Reynolds number $(U_m D/\nu)$
r_0^+	dimensionless tube radius $(r_0 u_*/\nu)$
U^+	dimensionless axial velocity (U/u_*)
y^+	dimensionless distance from the wall (yu_*/ν)
β_*	$\beta/90$
η	dimensionless distance from the wall (y/r_0)
$\Delta\eta$	dimensionless shift $(\Delta y/r_0)$

Subscripts

a	axial
c	core region
D	buffer zone
i	inside diameter
m	mean value
max	maximum value
t	tangential
v	vortex
w	wall

Some of the existing methods for enhancing heat transfer in a single-phase, fully developed turbulent flow in a round tube are one of the two types: (a) methods in which the inner surface of the tube is roughened, e.g. with repeated or helical ribbing, by sanding or with internal fins, and (b) methods in which a heat transfer promoter, e.g., a twisted tape, disk or streamlined shape is inserted into the tube.

It is well known that two or more of the existing techniques can be utilized simultaneously to produce an enhancement larger than that produced by only one technique. The combination of different techniques acting simultaneously is known as compound enhancement. Interactions between different enhancement methods contribute to greater values of the heat transfer coefficients compared to the sum of the corresponding values for the individual techniques used alone. Preliminary studies on compound passive enhancement technique of this kind were very encouraging. Some examples are: rough tube with a twisted tape [5] and grooved rough tube with a twisted tape [6].

The recent articles [7–10] report on an experimental investigation to see whether or not heat transfer can be enhanced by the multiplicative effect of a corrugated tube combined with a twisted tape. The geometrical characteristics of the corrugated tube and twisted tape insert are shown in 'Fig. 1'. Despite of the fact that comprehensive study was conducted on a variety of

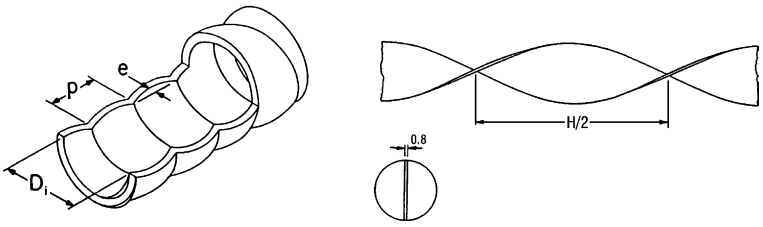

Fig. 1. Geometrical characteristics of a corrugated tube and twisted tape insert.

corrugated tubes combined with twisted tapes, a lack of sufficient knowledge about the flow mechanism does not permit the prediction of the friction factors and heat transfer coefficients by analytical methods.

The purpose of this paper is to create a simple mathematical model to predict the friction factor for the case of a fully developed single-phase turbulent flow in a corrugated tube combined with a twisted tape insert.

2. The mathematical model

The complicated nature of the geometry coupled with the initially unknown boundary layer effects makes an a priori analysis of the basic flow field an impossible task. The flow observations of the fully developed turbulent swirl flow induced by a twisted tape in a round smooth tube [11] showed that the flow field can be divided into two principal regions—a helicoidal core flow modified by secondary circulation effects and a twisting boundary layer flow. From hydrodynamic considerations the flow field is significantly influenced by a variety of effects: (1) the partitioning and blockage of the tube flow cross section by the tape, which results in higher flow velocities, (2) the helically twisting fluid motion has an effectively longer flow path, (3) secondary fluid motion generated by the tape twist is increased by the presence of the roughness elements [12].

When a corrugated tube is combined with a twisted tape insert the "wall roughness" has an effect simultaneously on the axial velocity, secondary fluid motion and the resulting swirl mixing. In order to predict friction losses in this assembly a model of the wall boundary layer should be formulated in addition to the core flow pattern. The model must reflect the influence of the "wall roughness", axial and tangential velocity components. Unfortunately, there exists no information on boundary layers of this type and the simplifying assumptions made in the subsequent analysis can be rationalized only by the absence of better information.

The approach presented here is an extension and modification of the idea of Smithberg and Landis [11] to predict friction factors for turbulent flow in a smooth tube with a twisted tape insert. It will be assumed that the turbulent flow is hydrodynamically fully developed. The physical properties of the fluid are constant while for a prescribed Reynolds number both the axial and tangential velocity distributions and the transport coefficients can be expressed as a function of the radial coordinate only. From physical considerations the flow can be considered as consisting of two regions of quite different nature—a helicoidal flow modified by secondary circulation effects and a twisting wall boundary layer flow. The helicoidal flow with its total velocity vector tangent at every point to a helix defined by the pitch of the twisted strip and the radial distance from the tube center line will result in a forced vortex motion in the tube cross section plan. This multiple vortex pattern will continuously mix wall boundary layer flow and should result in both increased friction losses and heat transfer [11].

To calculate the axial velocity component U^+, a "mixing-length" model for predicting fluid friction in "rough" pipes can be applied. This model was successfully implemented to predict the friction factor for turbulent flow in tubes with sand-grain roughness [13] and corrugated tubes [14]. The axial turbulent flow can be separated into two regions of different transport properties: (1) the wall region $0 \leqslant \eta \leqslant \eta_w$ where the whole influence of the wall is exhibited and (2) the core region $\eta_w < \eta \leqslant 1$ which is not influenced by the roughness of the wall. For the case considered the momentum equation yields the linear shear stress distribution as

$$\frac{\tau}{\tau_w} = 1 - \frac{y}{r_0} = 1 - \eta, \tag{1}$$

where the shear stress is assumed to satisfy the constitutive equation

$$\frac{\tau}{\tau_w} = \left(1 + \frac{\varepsilon_m}{\nu}\right)\frac{dU^+}{dy^+} = \left(1 + \frac{\varepsilon_m}{\nu}\right)\frac{1}{r_0^+}\frac{dU^+}{d\eta}. \tag{2}$$

For the wall region the eddy kinematic viscosity can be defined as

$$\frac{\varepsilon_m}{\nu}(\eta) = r_0^+\left(\frac{l^+}{r_0^+}\right)^2\frac{dU^+}{d\eta}, \quad 0 < \eta \leqslant \eta_w, \tag{3a}$$

where

$$l^+/r_0^+ = 0.4\eta\left(1 - \exp(-\eta r_0^+/26)\right). \tag{3b}$$

In Eq. (3) η_w is the unknown thickness of the wall region. The approach of Rotta developed in details for a rough plate [15] was used to insert corrections reflecting the influence of the roughness elements in Eq. (3). In this model the effect of the roughness is considered to be equivalent to a velocity jump over the viscous sublayer and it can be represented by a shift of the smooth wall flow velocity profile. For a flow over a rough wall the reference wall is shifted downward by an amount of Δy and it moves at a velocity of ΔU in a direction opposite to the direction of the main flow [15]. Here this quantity is represented by $\Delta\eta$.

Obviously, to calculate the axial velocity component $U^+(\eta)$ and the eddy kinematic viscosity $\varepsilon_m/\nu(\eta)$ one has to know the dependence of the dimensionless shift $\Delta\eta$ on the geometry of the corrugated tube. For this reason, it has been recently established an updated relationship between $\Delta\eta$, e/D_i, p/e, β_* and Re on the basis of the experimental information of 50 spirally and transversely corrugated tubes [7–9,16–20]. Despite of the fact that the corrugated tubes used are not exactly identical to the shape of the ridges, an attempt has been made to generalize this relationship including data of similar

corrugated tubes as much as possible. This relationship has been obtained through a procedure explained in details in [14]. It is well known from the study of Webb et al. [21] that the flow pattern in tubes with transverse-rib roughness depends on the dimensionless rib spacing p/e. The flow separates at the rib and reattaches six-eight rib heights downstream from the rib. In this regard, two correlations for $\Delta\eta$ have been obtained from the experimental data: one for $p/e > 9.0$ and another for $7.0 < p/e < 9.0$. These correlations can be presented in the forms

$$\Delta\eta = 90.31 Re^{-0.569}(e/D_i)^{0.732}\beta_*^{1.434}(p/e)^{-0.248}, \quad p/e > 9.0, \tag{4a}$$

$$\Delta\eta = 43.30 Re^{-0.476}(e/D_i)^{1.200}\beta_*^{2.500}(p/e)^{0.375}, \quad 7.0 \leqslant p/e \leqslant 9.0, \tag{4b}$$

in the ranges $8\times10^3 < Re < 6\times10^4$; $0.015 < e/D_i < 0.060$; $0.670 < \beta_* < 1.000$.

Thus, the wall roughness can be accounted for by formally replacing η by $(\eta + \Delta\eta)$ in Eqs. (1), (2) and (3). The thickness of the boundary layer η_w is not known a priori and it is calculated for a prescribed Reynolds number from the condition that at the boundary the eddy viscosity is a continuous function of the radial coordinate

$$(\varepsilon_m^+)_w = (\varepsilon_m^+)_c, \quad \eta = \eta_w. \tag{5}$$

In the core region, $\eta_w < \eta \leqslant 1$, the "mixing length" hypothesis is considered invalid and there will be no correction for the wall roughness. The eddy kinematic viscosity distribution is the same as in [13,22]

$$\frac{\varepsilon_m}{\nu}(\eta) = 0.07044 r_0^+\left(1-(1-\eta)^2\right)\left(1+2.345(1-\eta)^2\right), \quad \eta_w < \eta \leqslant 1. \tag{6}$$

Combining Eqs. (1)–(6), an initial value problem has to be solved:

$$\frac{dU^+}{d\eta} = 2[1-(\eta+\Delta\eta)]\left\{\frac{1}{r_0^+} + \left[\frac{1}{r_0^{+2}} + 4(1-(\eta+\Delta\eta))\frac{l^{+2}}{r_0^{+2}}\right]^{0.5}\right\}^{-1}, \quad 0 \leqslant \eta \leqslant \eta_w, \tag{7a}$$

$$\frac{dU^+}{d\eta} = (1-\eta)\left\{\frac{1}{r_0^+} + 0.07044\left[1-(1-\eta)^2\right] \times \left[1+2.345(1-\eta)^2\right]\right\}^{-1}, \quad \eta_w < \eta \leqslant 1, \tag{7b}$$

$$U^+ = 0, \quad \eta = 0, \tag{7c}$$

to determine the velocity $U^+(\eta)$, r_0^+ and η_w. For this purpose a continuity condition on ε_m/ν is imposed on $\eta = \eta_w$ and an iterative process is organized to converge on the value of r_0^+ [13,22].

The proposed wall boundary layer model assumes that the tangential velocity component is taken to vary linearly across the laminar sublayer and buffer zone, at a distance of $y_D^+ = 15$, and is given by

$$V_{t,D} = \frac{y}{y_D}(1-\eta_D)\frac{2\pi U_m}{H}r_0 = \frac{\eta}{\eta_D}(1-\eta_D)\frac{\pi U_m}{H/D_i}, \quad 0 \leqslant \eta \leqslant \eta_D, \tag{8}$$

which follows from the forced vortex relationship

$$V_t = \frac{2\pi U_m}{H}r = (1-\eta)\frac{\pi U_m}{H/D_i}, \quad \eta_D \leqslant \eta \leqslant 1. \tag{9}$$

In dimensionless forms, $V_{t,D}^+ = V_{t,D}/u_*$ and $V_t^+ = V_t/u_*$

$$V_{t,D}^+ = \frac{\eta}{\eta_D}(1-\eta_D)\frac{\pi U_m^+}{H/D_i} = \frac{\pi(1-\eta_D)}{\sqrt{f/2}(H/D_i)\eta_D}\eta, \quad 0 \leqslant \eta \leqslant \eta_D, \tag{10}$$

$$V_t^+ = (1-\eta)\frac{\pi U_m^+}{H/D_i} = \frac{\pi(1-\eta)}{\sqrt{f/2}(H/D_i)}, \quad \eta_D \leqslant \eta \leqslant 1. \tag{11}$$

This assumption is acceptable since for the most pitch-to-diameter ratios of practical interest the maximum tangential velocity at the outside of this region remains smaller than the axial velocity.

Following Smithberg and Landis [11], it is further assumed that the mechanical energy losses due to the axial flow, the tangential flow, and the vortex mixing may be added in the form of equivalent $\Delta p/\rho$ terms to define the overall friction factor

$$f = \frac{\Delta p_{tot}}{\rho}\frac{D_H}{2LU_m^2} = (\Delta p_a + \Delta p_t + \Delta p_v)\frac{D_H}{2L\rho U_m^2}, \tag{12}$$

where

$$f = f_a + f_t + f_v = f(Re_H). \tag{13}$$

The energy loss components can now be evaluated as follows.

For the axial component

$$\Delta p_a/\rho = f_a\frac{2LU_m^2}{D_H},$$

the friction factor f_a can easily be predicted from

$$f_a = 0.5\left[\int_0^1 (1-\eta)U^+(\eta)\,d\eta\right]^{-2} = f(Re_H), \tag{14}$$

once Eq. (7) are solved.

To verify the validity of the correction $\Delta\eta$, Eq. (4), in the case of corrugated tube acting alone, 120 friction factors have been calculated from Eq. (14) and compared

with the points obtained from the experimental program [7–9]. Fifty nine points (49.2%) showed a relative difference of less than ±10%, twenty six points (21.7%) have a difference of less than ±15%, nineteen points (15.8%) have a difference of less than ±20% and sixteen points (13.3%) have a difference of less than ±25%. Having in mind that the corrugated tubes [7–9,16–20] have not identical shapes of the ridges or ribs, this discrepancy should be considered as quite acceptable.

The tangential loss component is specified by the energy dissipation per unit mass to overcome the shear stress at the wall $(\tau_t)_w$ due to the solid core vortex

$$\dot{m}\frac{\Delta p_t}{\rho} = (\tau_t)_w A_w (V_t)_{r=r_0-y_D} \tag{15}$$

where the shear stress is considered to remain constant throughout the layer $y_D^+ \leqslant 15$ and can be evaluated from the assumed velocity distribution, Eq. (8) as

Table 1
Values of the characteristic parameters of the corrugated tubes

Tube	D_i/mm	e/mm	p/mm	β/°	e/D_i	p/e	β_*
3010	13.90	0.312	5.76	82.4	0.0224	18.46	0.916
3020	12.44	0.515	4.48	83.4	0.0414	8.70	0.927
3040	13.39	0.497	5.77	82.2	0.0371	11.61	0.913
3050	13.15	0.593	5.06	83.0	0.0451	8.53	0.922
3070	13.66	0.622	8.12	79.3	0.0456	13.05	0.881
4020	13.53	0.507	4.55	72.2	0.0375	8.97	0.802
4030	13.73	0.781	5.82	68.0	0.0569	7.45	0.755
4040	13.68	0.557	5.97	67.4	0.0407	10.73	0.749
4050	13.38	0.581	5.08	70.1	0.0434	8.74	0.779
2010	13.68	0.315	6.67	90.0	0.0230	21.17	1.000
2040	13.65	0.440	6.01	90.0	0.0322	13.66	1.000
2070	13.59	0.464	8.55	90.0	0.0341	18.43	1.000

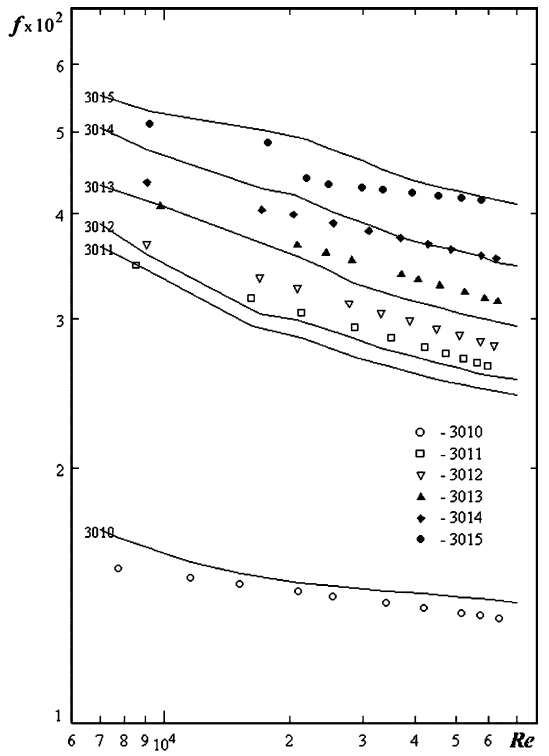

Fig. 2. Friction factor vs. Reynolds number. Comparison between computed and experimental results ($3010 - H/D_i = 0$; $3011 - H/D_i = 15.11$; $3012 - H/D_i = 12.09$; $3013 - H/D_i = 7.63$; $3014 - H/D_i = 5.76$; $3015 - H/D_i = 4.75$).

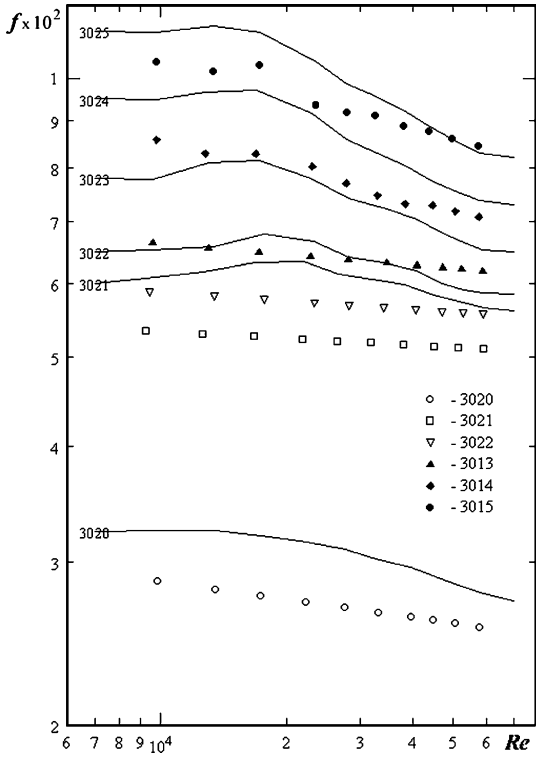

Fig. 3. Friction factor vs. Reynolds number. Comparison between computed and experimental results ($3020 - H/D_i = 0$; $3021 - H/D_i = 16.88$; $3022 - H/D_i = 13.50$; $3023 - H/D_i = 8.52$; $3024 - H/D_i = 6.43$; $3025 - H/D_i = 5.23$).

$$(\tau_t)_w = \mu\left(\frac{\partial V_{t,D}}{\partial y}\right)_{y=0} = \frac{2\mu}{D_i}\frac{\pi U_m}{H/D_i}\frac{1-\eta_D}{\eta_D}. \quad (16)$$

In Eq. (15), $\dot{m} = \rho U_m \frac{\pi D_H^2}{4}$; $A_w = \pi D_H L$; $(V_t)_{r=r_0-y_D} = (1-\eta_D)\frac{\pi U_m}{H/D_i}$.

After substitution in Eq. (15), it yields

$$\frac{\Delta p_t}{\rho} = \frac{8\nu\pi^2(1-\eta_D)^2 U_m L}{D_i\eta_D(H/D_i)^2 D_H} = 4f_t\frac{L}{D_H}\frac{U_m^2}{2} \quad (17)$$

and for the tangential component of the friction factor

$$f_t = \frac{4\pi^2(1-\eta_D)^2}{Re_H\eta_D(H/D_i)^2(D_i/D_H)} = f(Re_H), \quad (18)$$

where

$$\frac{D_i}{D_H} = \frac{\pi + 2(1-2e/D_i) - 2\delta/D_i}{\pi - 4\delta/D_i(1-2e/D_i)}. \quad (19)$$

The vortex mixing losses are derived by considering that the low velocity axial wall boundary layer fluid is carried into the center line causing a core retardation which is equivalent to an axial momentum exchange given by

$$\Delta p_v A_c = 2\int_0^{r_0} d\dot{m}(U_{max} - U), \quad (20)$$

where $d\dot{m} = \rho V_t L\, dr$ for half of the tube. Since the core flow velocities are nearly uniform, no allowance for boundary layer energy losses in the core has been accounted for. After introducing dimensionless variables it leads to

$$\Delta p_v\left[\frac{\pi D_i^2}{4} - \delta(D_i - 2e)\right] = 2\int_0^{y_v}\rho V_t L(U_{max} - U)\,dy = 2\rho L r_0 u_*^2\int_0^{\eta_v} V_t^+(U_{max}^+ - U^+)\,d\eta$$

and

$$\Delta p_v = \frac{4u_*^2\rho L}{\pi D_i\left[1 - \frac{4\delta}{\pi D_i}(1-2e/D_i)\right]}\int_0^{\eta_v} V_t^+(U_{max}^+ - U)\,d\eta = 2f_v\frac{L}{D_H}\rho U_m^2. \quad (21)$$

Thus, the component of the friction factor f_v, taking account of the total vortex mixing loss, is

$$f_v = \frac{2(f/2)}{\pi(D_i/D_H)\left[1 - \frac{4\delta}{\pi D_i}(1-2e/D_i)\right]}\int_0^{\eta_v} V_t^+(U_{max}^+ - U^+)\,d\eta = f(Re_H). \quad (22)$$

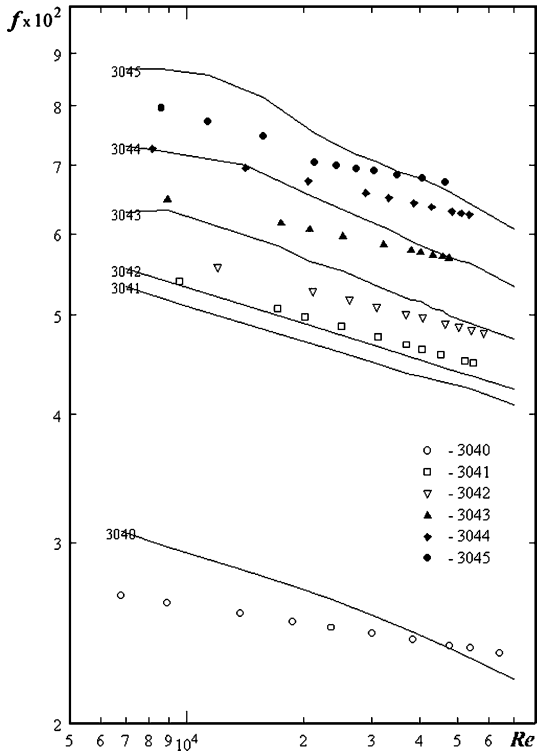

Fig. 4. Friction factor vs. Reynolds number. Comparison between computed and experimental results ($3040 - H/D_i = 0$; $3041 - H/D_i = 15.68$; $3042 - H/D_i = 12.54$; $3043 - H/D_i = 7.91$; $3044 - H/D_i = 5.97$; $3045 - H/D_i = 4.85$).

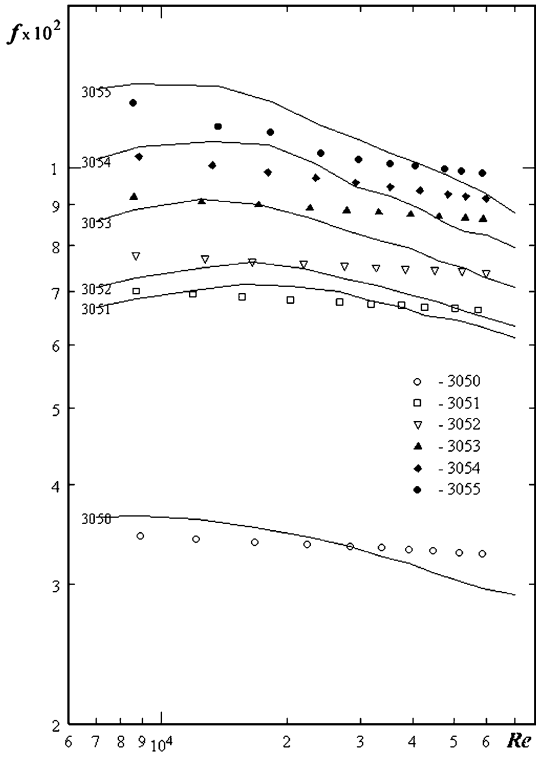

Fig. 5. Friction factor vs. Reynolds number. Comparison between computed and experimental results ($3050 - H/D_i = 0$; $3051 - H/D_i = 15.97$; $3052 - H/D_i = 12.77$; $3053 - H/D_i = 8.06$; $3054 - H/D_i = 6.08$; $3055 - H/D_i = 4.94$).

The distance η_v is defined by the assumption that the surface roughness increases additionally the vortex mixing of the boundary layer in the vicinity of the ridges. In this regard, it is expected that the distance η_v should be greater than η_D and to depend on the geometry of the roughness elements and Reynolds number. For this reason, the value of η_v is suggested to be calculated as $\eta_v = \eta_D + \Delta\eta$ but no greater than e/D_i for the case $p/e \geqslant 9.0$ and $\eta_v = 4\eta_D + \Delta\eta$, for the case $7.0 \leqslant p/e \leqslant 9.0$. The latter is also restricted in the limits $0.5e/D_i \leqslant \eta_v \leqslant 1.5e/D_i$. Thus, the integral in Eq. (22) can be split into two parts

$$f_v = \frac{2(f/2)}{\pi(D_i/D_H)\left[1-\frac{4\delta}{\pi D_i}(1-2e/D_i)\right]} \times \left\{ \frac{(1-\eta_D)\pi}{\eta_D\sqrt{f/2}(H/D_i)} \int_0^{\eta_D} (U^+_{max} - U^+)\eta\,d\eta + \frac{\pi}{\sqrt{f/2}(H/D_i)} \int_{\eta_D}^{\eta_v} (U^+_{max} - U^+)(1-\eta)\,d\eta \right\}. \quad (23)$$

For the velocity distribution V_t^+, in the regions $0 \leqslant \eta \leqslant \eta_D$ and $\eta_D \leqslant \eta \leqslant \eta_v$, Eqs. (8) and (9) are respectively used. Finally, Eq. (23) yields

$$f_v = \frac{2\sqrt{(f/2)}}{(H/D_i)(D_i/D_H)\left[1-\frac{4\delta}{\pi D_i}(1-2e/D_i)\right]} \times \left\{ \frac{(1-\eta_D)}{\eta_D} \int_0^{\eta_D} (U^+_{max} - U^+)\eta\,d\eta + \int_{\eta_D}^{\eta_v} (U^+_{max} - U^+)(1-\eta)\,d\eta \right\} = f(Re_H). \quad (24)$$

Accordingly, the overall friction factor f can be obtained from Eqs. (13), (14), (18) and (24) by an iterative procedure organized to converge on the value of r_0^+. The correlated overall friction factor f and Reynolds number are related to the hydraulic diameter, D_H. To recalculate these results with respect to the inside diameter of the tube D_i, the following transformations should be fulfilled

$$Re_i = Re_H \frac{\pi + 2(1-2e/D_i) - 2\delta/D_i}{\pi}, \quad (25)$$

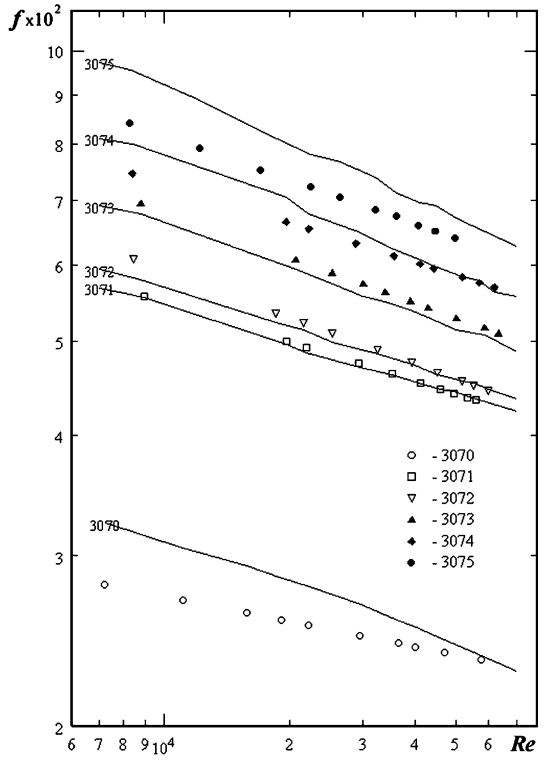

Fig. 6. Friction factor vs. Reynolds number. Comparison between computed and experimental results ($3070 - H/D_i = 0$; $3071 - H/D_i = 15.38$; $3072 - H/D_i = 12.31$; $3073 - H/D_i = 7.77$; $3074 - H/D_i = 5.86$; $3075 - H/D_i = 4.76$).

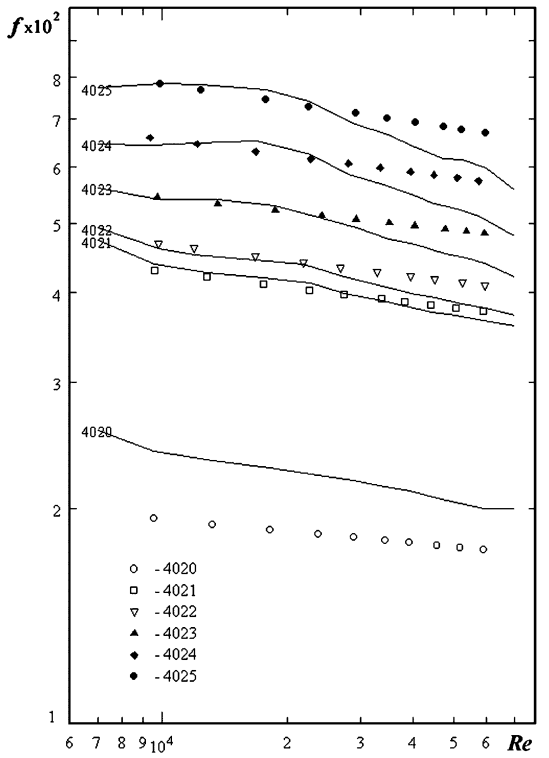

Fig. 7. Friction factor vs. Reynolds number. Comparison between computed and experimental results ($4020 - H/D_i = 0$; $4021 - H/D_i = 15.52$; $4022 - H/D_i = 12.42$; $4023 - H/D_i = 7.83$; $4024 - H/D_i = 5.91$; $4025 - H/D_i = 4.80$).

$$f(Re_i) = f(Re_H)\frac{1 + 2(1 - 2e/D_i - \delta/D_i)/\pi}{\left[1 - \frac{4}{\pi}\frac{\delta}{D_i}(1 - 2e/D_i)\right]^3}. \quad (26)$$

The model discussed here comprises the following cases concerning the calculation of the friction factor in a fully developed turbulent flow in a pipe:

(a) if $\Delta\eta = 0$ and $H/D_i = 0$—the model can be used to calculate the friction factors in a smooth pipe [22];
(b) if $\Delta\eta > 0$ and $H/D_i = 0$—the model calculates the friction factors for a corrugated pipe [14];
(c) if $\Delta\eta = 0$ and $H/D_i > 0$—the model calculates the friction factors for a smooth pipe combined with a twisted tape insert [23];
(d) if $\Delta\eta > 0$ and $H/D_i > 0$—the model calculates the friction factors for a corrugated pipe combined with a twisted tape insert.

3. Results and discussion

The Fanning friction factors calculated by the approach outlined were compared with 570 experimental points obtained from 57 tested corrugated tubes combined with twisted tape inserts. The values of the geometrical parameters of the corrugated tubes are presented in Table 1. Three hundred and ninety five points (69.3%) showed a relative difference of less than ±10%, one hundred and five points (18.4%) have a relative difference within ±(10–15)%; fifty one points (8.9%) have a relative difference within ±(15–20)%. Only 19 points have a relative difference greater than ±20%. The numerical results for the friction factors together with the experimental data of some spirally corrugated tubes combined with twisted tape inserts are presented in 'Figs. 2–13'. Taking into account the experimental error in the measurements, this agreement should be considered as fairly acceptable. Because of the lack of other experimental data of this kind (for corrugated tubes with twisted tape inserts) an attempt to verify the model has been made with the study of Bergles et al. [5] where isothermal and heated friction factors for straight flow and swirl flow in rough tubes with twisted tape inserts were reported, 'Fig. 14'. Comparison with generalized Moody friction factor chart [24] has suggested an equivalent sand grain roughness of $e_s/D_i = 0.005$–0.015

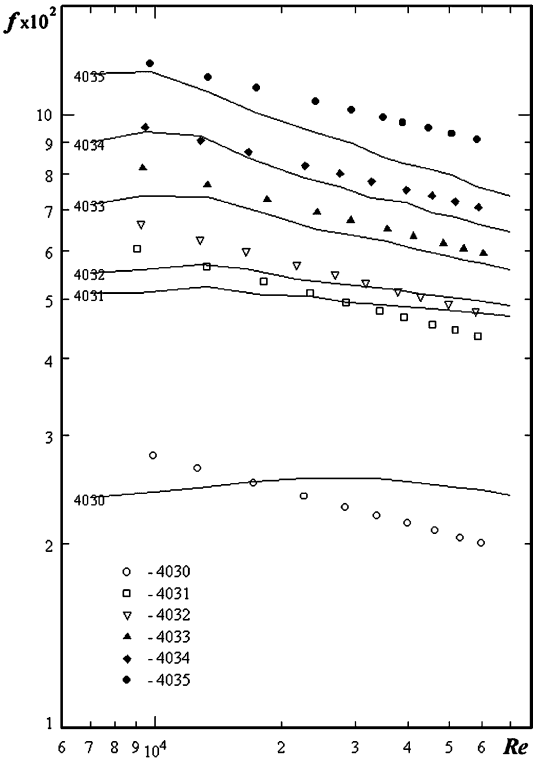

Fig. 8. Friction factor vs. Reynolds number. Comparison between computed and experimental results ($4030 - H/D_i = 0$; $4031 - H/D_i = 15.30$; $4032 - H/D_i = 12.24$; $4033 - H/D_i = 7.72$; $4034 - H/D_i = 5.83$; $4035 - H/D_i = 4.73$).

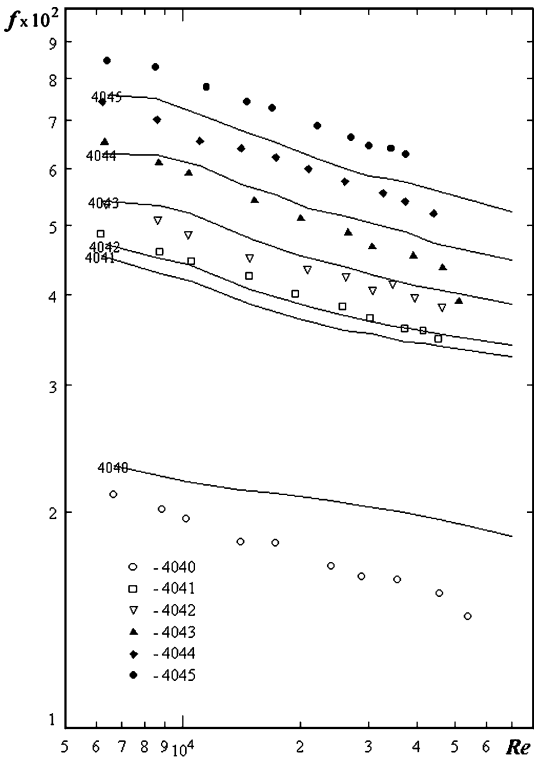

Fig. 9. Friction factor vs. Reynolds number. Comparison between computed and experimental results ($4040 - H/D_i = 0$; $4041 - H/D_i = 15.35$; $4042 - H/D_i = 12.28$; $4043 - H/D_i = 7.75$; $4044 - H/D_i = 5.85$; $4045 - H/D_i = 4.75$).

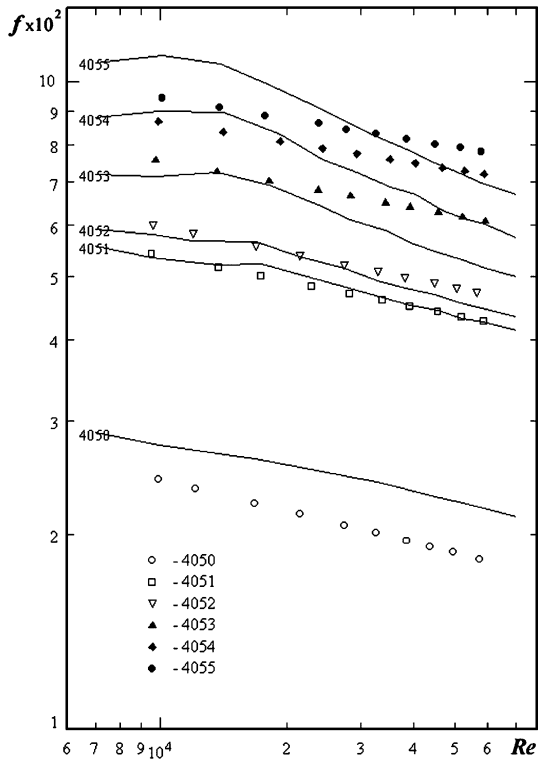

Fig. 10. Friction factor vs. Reynolds number. Comparison between computed and experimental results ($4050 - H/D_i = 0$; $4051 - H/D_i = 15.69$; $4052 - H/D_i = 12.55$; $4053 - H/D_i = 7.92$; $4054 - H/D_i = 5.98$; $4055 - H/D_i = 4.86$).

[5]. Giving different values of e_s/D_i for different Reynolds numbers the friction factors have been calculated through the model discussed here. In this case, the turbulent flow in rough tubes (sand grain roughness) has been simulated through replacing the dimensionless shift $\Delta\eta$ with [13,15]

$$\Delta\eta = \frac{0.9}{r_0^+}\left(\sqrt{e_s^+} - e_s^+ \exp(-e_s^+/6)\right). \quad (27)$$

As can be seen from 'Fig. 14', the agreement between predicted (solid line) and experimental data [5] is fairly good.

4. Conclusions

The results of the present study can be summarized as follows:

(1) A simple mathematical model has been created to predict the friction factors for the case of a fully developed turbulent flow in a spirally corrugated tube combined with a twisted tape insert which is an ex-

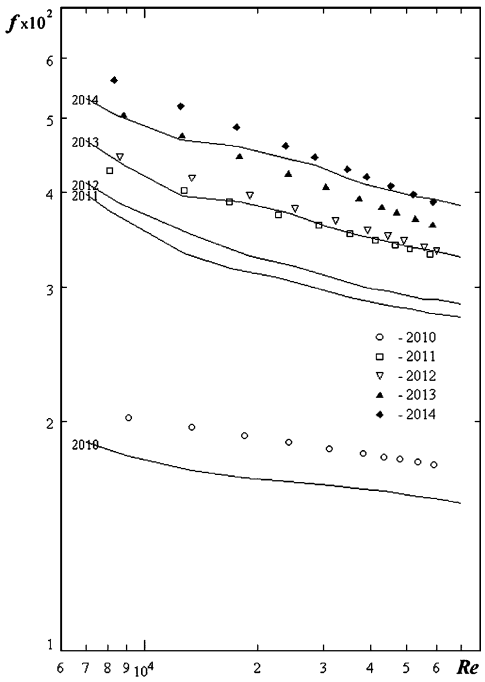

Fig. 11. Friction factor vs. Reynolds number. Comparison between computed and experimental results ($2010 - H/D_i = 0$; $2011 - H/D_i = 15.35$; $2012 - H/D_i = 12.28$; $2013 - H/D_i = 7.75$; $2014 - H/D_i = 5.85$).

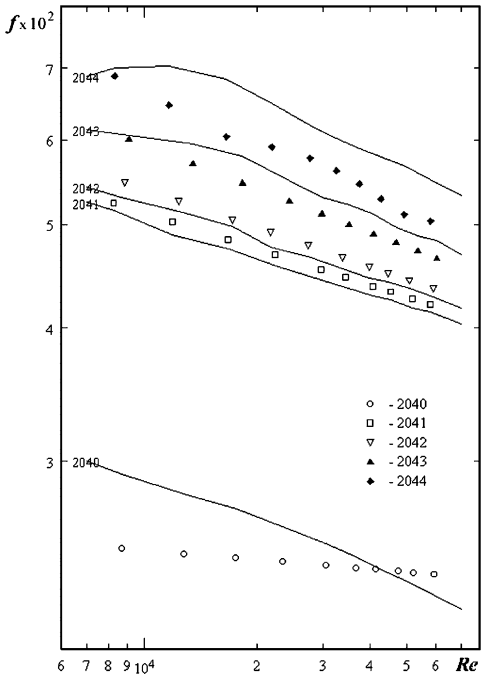

Fig. 12. Friction factor vs. Reynolds number. Comparison between computed and experimental results ($2040 - H/D_i = 0$; $2041 - H/D_i = 15.38$; $2042 - H/D_i = 12.30$; $2043 - H/D_i = 7.76$; $2044 - H/D_i = 5.86$).

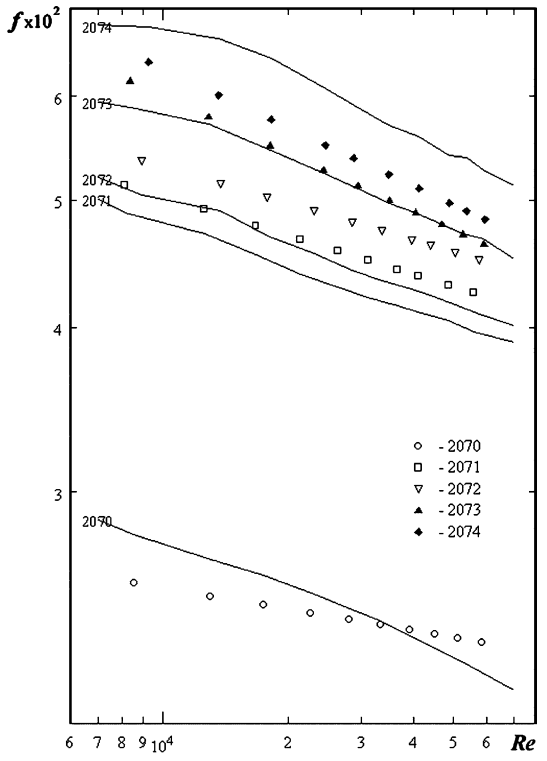

Fig. 13. Friction factor vs. Reynolds number. Comparison between computed and experimental results ($2070 - H/D_i = 0$; $2071 - H/D_i = 15.45$; $2072 - H/D_i = 12.36$; $2073 - H/D_i = 7.80$; $2074 - H/D_i = 5.89$).

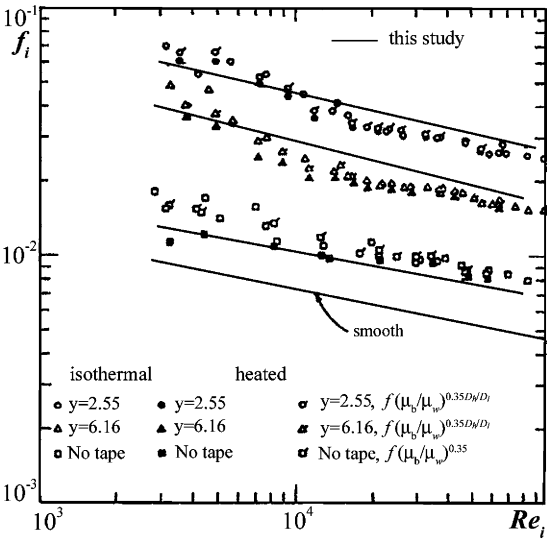

Fig. 14. Friction factor vs. Reynolds number. Comparison between computed and experimental results of [5] ($y = 0.5H/D_i$).

tension and modification of the idea of Smithberg and Landis to predict friction factors for a turbulent flow in a smooth tube with a twisted tape insert.

(2) The model reflects the influence of the "wall roughness" on the axial velocity, secondary fluid motion and the resulting swirl flow.

(3) The calculated friction factors have been compared with 570 experimental points obtained from 57 tubes tested. To verify the validity of the model for another type of "wall roughness" the calculated friction factors for turbulent flow in rough tubes (sand grain roughness) with twisted tape inserts have been compared to the experimental data of Bergles et al. [5]. The agreement between predicted and experimental data is fairly good.

(4) The model comprises the possibilities to predict the friction factors in the cases of a turbulent flow in a smooth pipe; a smooth pipe with a twisted tape insert; a corrugated tube and a corrugated tube combined with a twisted tape insert.

References

[1] A.E. Bergles, Techniques to augment heat transfer, in: Handbook of Heat Transfer Applications, vol. 3–1, 1985, pp. 3–80, Chapter 3.

[2] A.E. Bergles, Some perspectives on enhanced heat transfer second generation heat transfer technology, Trans. ASME, J. Heat Transfer 110 (1988) 1082–1096.

[3] A.E. Bergles, Heat transfer enhancement—the encouragement and accommodation of high heat fluxes, Trans. ASME, J. Heat Transfer 119 (1997) 8–19.

[4] C.A. Balaras, A review of augmentation techniques for heat transfer surfaces in single-phase heat exchangers, Energy 15 (10) (1990) 899–906.

[5] A.E. Bergles, R.A. Lee, B.B. Mikic, Heat transfer in rough tubes with tape-generated swirl flow, Trans. ASME, J. Heat Transfer 91 (1969) 443–445.

[6] H. Usui, Y. Sano, K. Iwashita, A. Isozaki, Enhancement of heat transfer by a combination of an internally grooved rough tube and a twisted tape, Int. J. Chem. Eng. 26 (1) (1986) 97–104.

[7] V.D. Zimparov, Enhancement of heat transfer by a combination of three-start spirally corrugated tubes with a twisted tape, Int. J. Heat Mass Transfer 44 (2001) 551–574.

[8] V.D. Zimparov, Enhancement of heat transfer by a combination of a single-start spirally corrugated tubes with a twisted tape, Exp. Thermal Fluid Sci. 25 (2002) 535–546.

[9] V.D. Zimparov, V.M. Petkov, Compound heat transfer augmentation by a combination of spirally corrugated tubes with a twisted tape, in: Proceedings of the 1st International Conference of Heat Transfer, Fluid Mechanics and Thermodynamics, vol. 1, Kruger National Park, South Africa, 2002, pp. 547–552.

[10] V.D. Zimparov, V.M. Petkov, Compound heat transfer enhancement by a combination of spirally corrugated tubes

with a twisted tape, in: Proceedings 12th International Heat Transfer Conference, vol. 4, Grenoble, France, 2002, pp. 153–158.
[11] E. Smithberg, F. Landis, Friction and forced convection heat transfer characteristics in tubes with twisted tape swirl generators, Trans. ASME, J. Heat Transfer 86 (1964) 39–49.
[12] R.M. Manglik, A.E. Bergles, Heat transfer and pressure drop correlations for twisted-tape inserts in isothermal tubes: Part I—Laminar flows, Trans. ASME, J. Heat Transfer 115 (1993) 881–889.
[13] N.L. Vulchanov, V.D. Zimparov, Stabilized turbulent fluid friction and heat transfer in circular tubes with internal sand type roughness at moderate Prandtl numbers, Int. J. Heat Mass Transfer 32 (1) (1989) 29–34.
[14] N.L. Vulchanov, V.D. Zimparov, Heat transfer and friction characteristics of spirally corrugated tubes for power plant condensers—2. A mixing-length model for predicting fluid friction and heat transfer, Int. J. Heat Mass Transfer 34 (9) (1991) 2199–2206.
[15] T. Cebeci, A.M.O. Smith, Analysis of turbulent boundary layers, Academic Press, New York, 1974.
[16] V.D. Zimparov, N.L. Vulchanov, L.B. Delov, Heat transfer and friction characteristics of spirally corrugated tubes for power plant condensers. Part 1: experimental investigation and performance evaluation, Int. J. Heat Mass Transfer 34 (1991) 2187–2197.
[17] J.G. Withers, Tube-side heat transfer and pressure drop for tubes having helical internal ridging with turbulent/transitional flow of single-phase fluid. Part 1: single-helix ridging, Heat Transfer Eng. 1 (1980) 48–58.
[18] H.M. Li, K.S. Ye, Y.K. Tan, S.J. Deng, Investigation on tube side flow visualisation, friction and heat transfer characteristics of helical ridging tubes, in: Proceedings 7th International Heat Transfer Conference, vol. 3, Munich, 1982, pp. 75–80.
[19] Anon, YIA Heat Exchanger Tubes: Design data for horizontal roped tubes in steam condensers, Technical Memorandum 3, Yorkshire Imperial Alloys, Leeds, UK, 1982.
[20] E.K. Kalinin, G.A. Dreitser, S.A. Yarkho, Heat Transfer Enhancement in Channels, Mashinostroenie, Moscow, 1990 (in Russian).
[21] R.L. Webb, E.R.G. Eckert, R.J. Goldstein, Heat transfer and friction in tubes with repeated-rib roughness, Int. J. Heat Mass Transfer 14 (1971) 601–617.
[22] M.D. Mikhailov, N.L. Vulchanov, V.D. Zimparov, Computation of stabilized turbulent fluid flow and heat transfer in circular smooth pipes for moderate Prandtl numbers. Part 1. Fluid flow and eddy diffusivity, Bulgarian Academy of Sciences, Theor. Appl. Mech., Year XVI 2 (1985) 55–59.
[23] V.D. Zimparov, A mathematical model to predict fluid friction for turbulent in-tube flow with twisted tape inserts, Journal of TU-Gabrovo 27 (2003) 3–8.
[24] L.F. Moody, Friction factors for pipe flow, Trans. ASME 66 (1944) 671–684.